Progress In Electromagnetics Research, Vol. 115, 461–475, 2011

ON THE TAPERED OPTICAL FIBERS WITH RADIALLY ANISOTROPIC LIQUID CRYSTAL CLAD

P. K. Choudhury

Institute of Microengineering and Nanoelectronics (IMEN)
Universiti Kebangsaan Malaysia
UKM, Bangi, Selangor 43600, Malaysia

W. K. Soon

Pepperl+Fuchs (MFG) Pte Ltd.
P+F Building, 18 Ayer Rajah Crescent
Singapore 139942, Singapore

Abstract—The paper presents an analytical investigation of a tapered core optical fiber of which the outermost section is loaded with radially anisotropic liquid crystal. The analyses are dealt with transverse modes supported in the fiber structure followed by the relative distribution of power in the different fiber sections. Preliminary dispersion characteristics of the guide are also illustrated. The results demonstrate that the TE modes transport very large amount of power in the outermost liquid crystal region — the criteria much useful for fiber optic sensing and field coupling devices.

1. INTRODUCTION

Among the complex forms of waveguides, studies related to several varieties of them in respect of either the structure or the materials used have appeared in the literature describing their certain technological applications [1–13]. Liquid crystal fibers exhibit polarization anisotropy, which makes them of much technological interest and useful for many optical applications [14–16]. Investigators have reported such fibers with liquid crystals filled in the core/clad regions with varieties of material distributions. It is interesting to note that the macroscopic optical properties of liquid crystals can be manipulated by suitably

Received 1 March 2011, Accepted 11 April 2011, Scheduled 13 April 2011
Corresponding author: Pankaj Kumar Choudhury (pankaj@ukm.my).

applying the external electrical fields [17, 18], because liquid crystals present very large electro-optic effect. This feature essentially remains of promising use in optical sensing.

The anisotropy in liquid crystal fibers may be of two types — i.e., radial and azimuthal; many investigations on the former one have not appeared in the literature. The present report aims to emphasize the radially anisotropic behaviour of liquid crystal, which may generally be obtained after inserting the liquid crystal into a capillary tube coated with N, N-dimethyl-N-octadecyl-3-aminopropyltrimethoxysilyl chloride (DMOAP) [19]. In this connection, it would be of worth to state that the technique to prepare a fiber with liquid crystal clad is just based on deriving the same from the usually available fiber. The section of fiber length, where the liquid crystal clad is needed, can be etched to remove the original clad, and the same section can be coated with DMOAP to achieve homotropical alignment of the liquid crystal directors on the boundary. The radial configuration of the liquid crystal can be obtained by capillary action after inserting the treated fiber section into a DMOAP coated capillary tube with an inner diameter larger than the fiber core.

Following this, an investigation is carried out that deals with a liquid crystal fiber with the outermost clad section made of radially anisotropic liquid crystal. Further, the fiber geometry is taken to be tapered in the longitudinal direction as tapered fibers are proved to be of immense use in optical sensing and other *all optical* applications.

Thus, the present communication takes into account an amalgamation of features in respect of fiber geometry and the material — the former one relates to the tapered structure [20–23] and the latter one to the radially anisotropic outermost liquid crystal clad. This is done in order to observe the effect on the propagation of power in the liquid crystal section. Maxwell's equations are implemented for a rigorous analysis of the low order TE and TM modes, and the illustrations are made of the power sustained in the three regions of the fiber along the tapered length. Though the liquid crystal fibers with radial anisotropies have also been reported before by Choudhury and Yoshino [24, 25], a blend of liquid crystal material and tapered structure is observed to yield a substantial amount of power belonging to the outermost liquid crystal region — a much desirable aspect required for optical sensing applications. Preliminary investigations in respect of the transverse electric properties of tapered liquid crystal fibers were presented earlier by the authors; the present paper incorporates the transverse magnetic properties as well [26], and the comparative analysis of the two cases.

2. ANALYTICAL TREATMENT

We consider a liquid crystal tapered fiber, wherein the (infinitely extended) outermost clad is filled with radially anisotropic liquid crystal having the ordinary and the extraordinary refractive index (RI) values as n_o and n_e, respectively. The fiber core and the inner clad sections are homogeneous, isotropic and non-magnetic dielectrics with their respective RI values as n_1 and n_2 (with $n_1 > n_2$). In this connection, we have to state that, although the technique to prepare a liquid crystal clad fiber is described as above, for the sake of simplicity of the analytical treatment, the outermost liquid crystal section is considered as extended infinitely. The longitudinal view of the fiber under consideration is shown in Fig. 1, where the tapered nature of the structure is explicitly shown, as governed by

$$R(z) = R_o - \frac{z}{L}(R_o - R_i) \tag{1}$$

with R_i and R_o as the radius of the input and the output ends of the tapered section, respectively, of length L. As such, the principal axis of the fiber coincides with the z-axis, and the extraordinary principal axis has a radial orientation. The liquid crystal clad region possesses the RI distribution as

$$n_R = n_e \quad \text{and} \quad n_\phi = n_z \quad \text{with} \quad n_e > n_1 > n_2 > n_o.$$

This is illustrated in Figs. 2(a) and 2(b). Further, The region with $z < z_i$ ($= 0$, as considered in our analysis) corresponds to the fiber pigtail whereas those with $z > z_o$ ($= L$) to the expanded cylindrical section.

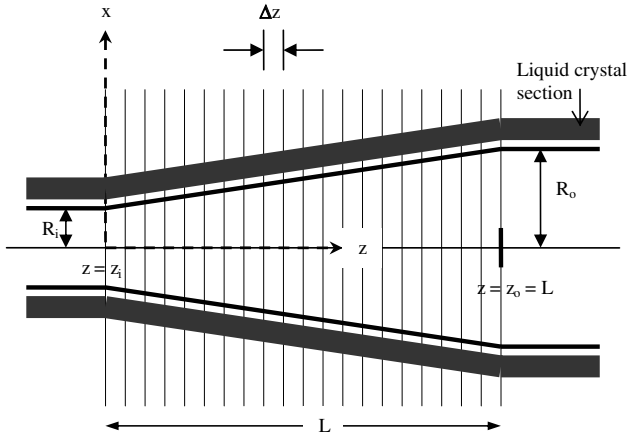

Figure 1. Tapered section of the liquid crystal fiber with split steps.

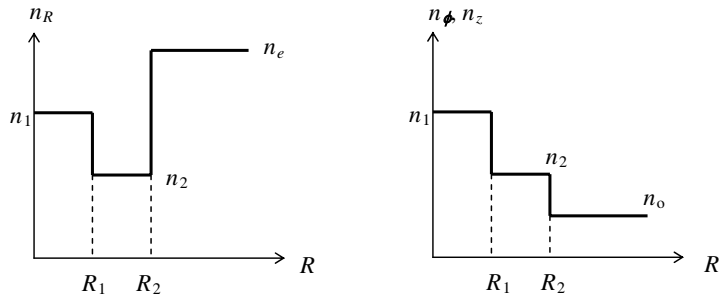

Figure 2. Spatial RI distribution pattern of the fiber.

For the electromagnetic (EM) propagation in the fiber of Fig. 1, the propagation constant (say β) will not be a constant. Instead, it remains a z-dependent quantity, which stimulates one to consider β in the form of a Taylor series expansion [27]

$$\beta \approx \beta_0 + \left(\frac{\partial \beta}{\partial z}\right) z \tag{2}$$

under the assumption of a small variation of the fiber core radius with z. In Eq. (2), β_0 is the axial component of the propagation vector at the origin $z = 0$.

Under the assumption of cylindrical polar coordinates (R, ϕ, z), we consider the time t-harmonic and the axis z-harmonic electric/magnetic fields, and the coupled wave equations for the transverse EM field components [28]. We take into account the low order modes, and it can then be stated that there will be only one non-zero transverse E-field component e_ϕ for the transverse electric TE_{01} mode, and only one non-zero component e_R for the transverse magnetic TM_{01} mode; both these components will be independent of the coordinate ϕ. Thus, for the TE_{01} mode, we have $e_R = 0$ and $\partial e_\phi / \partial \phi = 0$, and for the TM_{01} mode, $e_\phi = 0$ and $\partial e_R / \partial \phi = 0$. Under the circumstances, the wave equations for the TE and the TM modes may be presented as

$$\frac{\partial^2 e_\phi}{\partial R^2} + \frac{1}{R}\frac{\partial e_\phi}{\partial R} + \left(k_0^2 n_\phi^2 - \beta^2 - \frac{1}{R^2}\right) e_\phi = 0 \tag{3}$$

and

$$\frac{\partial^2 e_R}{\partial R^2} + \frac{1}{R}\frac{\partial e_R}{\partial R} + \left\{\left(k_0^2 n_R^2 - \beta^2\right)\left(\frac{n_z}{n_R}\right)^2 - \frac{1}{R^2}\right\} e_R = 0, \tag{4}$$

respectively. Using Eqs. (3) and (4), it can be shown that the non-zero

field components in the case of TE_{01} mode will be

$$H_R = -\frac{\beta}{\omega\mu_0} e_\phi \exp\{j(\omega t - \beta z)\} \text{ with } H_R = h_R \exp\{j(\omega t - \beta z)\} \quad (5a)$$

and

$$H_z = \frac{j}{\omega\mu_0}\left(\frac{\partial e_\phi}{\partial R} + \frac{e_\phi}{R}\right)\exp\{j(\omega t - \beta z)\} \text{ with } H_z = h_z \exp\{j(\omega t - \beta z)\}, \quad (5b)$$

and those in the case of TM_{01} mode will assume the form

$$E_z = -j\frac{n_e^2}{\beta n_o^2}\left(\frac{\partial e_R}{\partial R} + \frac{e_R}{R}\right)\exp\{j(\omega t - \beta z)\} \quad (6a)$$

and

$$H_\phi = n_R^2 e_R \frac{\omega\varepsilon_0}{\beta}\exp\{j(\omega t - \beta z)\}. \quad (6b)$$

In Eqs. (5) and (6), ω is the angular frequency in the non-magnetic unbounded medium, μ_0 is the free-space permeability and β is the propagation constant along the optical axis. Further, R and β are governed throughout by Eqs. (1) and (2), respectively.

Now, considering Eqs. (3) and (5), the electric/magnetic field components in the different fiber sections may be deduced [19, 20], based on which the dispersion relation for the guide may be obtained by implementing the boundary conditions, which will ultimately yield the frequency behavior of the tapered fiber with liquid crystal clad. The matrix obtained after matching the fields in different regions may be written in abbreviated form as $\Delta_{TE} = 0$. The explicit form of the matrix is not shown here owing to its length. Further, based on the electric/magnetic field components, expressions for the power transmitted by the TE_{01} modes in the different fiber sections may be finally obtained as

$$P_c = \Psi\left(\frac{\pi}{\omega\mu_0}\right)\left\{\int_0^{R_1}(J_1(uR))^2\,dR + u\int_0^{R_1} RJ_1(uR)J_1'(uR)dR\right\} \quad (7)$$

$$P_{ic} = \Psi\left(\frac{\pi}{\omega\mu_0}\right)\left[\left\{\int_{R_1}^{R_2}(I_1(vR))^2\,dR + v\int_{R_1}^{R_2} RI_1(vR)I_1'(\gamma_2 R)dR\right\}\right.$$

$$\left.\times\left\{\frac{vK_1'(vR_1)J_1(uR_1) + K_1(vR_1)\left(\frac{1}{R_1}(J_1(uR_1) - J_1(uR_1)) - uJ_1'(uR_1)\right)}{vK_1'(vR_1)I_1(vR_1) + K_1(vR_1)\left(\frac{1}{R_1}(I_1(vR_1) - K_1(vR_1)) - vI_1'(vR_1)\right)}\right\}^2\right.$$

$$+\left\{\frac{J_1(uR_1)\left(vI_1'(vR_1)+\frac{1}{R_1}(K_1(vR_1)-I_1(vR_1))\right)-uJ_1'(uR_1)I_1(vR_1)}{K_1(vR_1)\left(vI_1'(vR_1)+\frac{1}{R_1}(K_1(vR_1)-I_1(vR_1))\right)-vK_1'(vR_1)I_1(vR_1)}\right\}^2$$

$$\times\left\{\int_{R_1}^{R_2}(K_1(vR))^2\,dR+v\int_{R_1}^{R_2}RK_1(vR)K_1'(vR)dR\right\}$$

$$+\left\{\frac{vK_1'(vR_1)J_1(uR_1)+K_1(vR_1)\left(\frac{1}{R_1}(J_1(uR_1)-J_1(uR_1))-uJ_1'(uR_1)\right)}{vK_1'(vR_1)I_1(vR_1)+K_1(vR_1)\left(\frac{1}{R_1}(I_1(vR_1)-K_1(vR_1))-vI_1'(vR_1)\right)}\right\}$$

$$\times\left\{\frac{J_1(uR_1)\left(vI_1'(vR_1)+\frac{1}{R_1}(K_1(vR_1)-I_1(vR_1))\right)-uJ_1'(uR_1)I_1(vR_1)}{K_1(vR_1)\left(vI_1'(vR_1)+\frac{1}{R_1}(K_1(vR_1)-I_1(vR_1))\right)-vK_1'(vR_1)I_1(vR_1)}\right\}$$

$$\times\left\{2\int_{R_1}^{R_2}K_1(vR)I_1(vR)dR+v\int_{R_1}^{R_2}RK_1(vR)I_1'(vR)dR\right.$$

$$\left.+\,v\int_{R_1}^{R_2}RI_1(vR)K_1'(vR)dR\right\}\Bigg] \tag{8}$$

$$P_{oc}=\Psi\left(\frac{\pi}{\omega\mu_0}\right)\left[\frac{1}{K_1(wR_2)}\{I_1(vR_1)\right.$$

$$\left(\frac{vK_1'(vR_1)J_1(uR_1)+K_1(vR_1)\left(\frac{1}{R_1}(J_1(uR_1)-J_1(uR_1))-uJ_1'(uR_1)\right)}{vK_1'(vR_1)I_1(vR_1)+K_1(vR_1)\left(\frac{1}{R_1}(I_1(vR_1)-K_1(vR_1))-vI_1'(vR_1)\right)}\right)$$

$$+K_1(\nu R_2)$$

$$\left.\left(\frac{J_1(uR_1)\left(vI_1'(vR_1)+\frac{1}{R_1}(K_1(vR_1)-I_1(vR_1))\right)-uJ_1'(uR_1)I_1(vR_1)}{K_1(vR_1)\left(vI_1'(vR_1)+\frac{1}{R_1}(K_1(vR_1)-I_1(vR_1))\right)-vK_1'(vR_1)I_1(vR_1)}\right)\right\}\Bigg]^2$$

$$\left[\int_{R_2}^{\infty}\{K_1(wR)\}^2\,dR+w\int_{R_2}^{\infty}RK_1(wR)K_1'(wR)dR\right] \tag{9}$$

Eqs. (7), (8) and (9), respectively, represent the power transported by the TE modes through the liquid crystal tapered fiber core, its inner dielectric clad and the outermost liquid crystal clad sections. Here, Ψ is a constant which can be determined by normalization condition considering the input power. Also, $J(\bullet)$, $K(\bullet)$ and $I(\bullet)$ are

Bessel and the modified Bessel functions, and the prime represents the differentiation with respect to the argument of the function. Further, the quantities u, v and w are, respectively, defined as

$$u = \sqrt{n_1^2 k_0^2 - \beta^2}, \tag{10a}$$

$$v = \sqrt{\beta^2 - n_2^2 k_0^2}, \tag{10b}$$

$$\text{and} \quad w = \sqrt{\beta^2 - n_o^2 k_0^2} \tag{10c}$$

with $k_0 = 2\pi/\lambda_0$; λ_0 being the free-space wavelength. The total power P_t transmitted by the TE_{01} mode through the fiber will then be the sum of the power carried individually through the different fiber sections.

At this point, it is to be pointed out that the quantities R_1 and R_2 in Eqs. (7)–(9) represent the localized values of the core and the inner clad radii of the fiber under consideration. This is because we implemented the split-step method [21–23] to treat the tapered extension of the fiber along the longitudinal direction. Moreover, as stated before, the values of β are throughout governed by Eq. (2).

Again considering Eqs. (4) and (6), the electric/magnetic field components in the different fiber sections may also be found out [19], which will ultimately yield the dispersion equation for this case, and may by written in abbreviated form as $\Delta_{TM} = 0$ to illustrate the frequency behavior of the tapered section. The explicit form of the dispersion equation is not presented in the text owing to its formidable size. The expressions of power transported by the TM_{01} modes in the different fiber sections may also be deduced on the basis of the electric/magnetic field components. Finally, the expressions will assume the forms as follows:

$$p_c = \Xi (1+\Theta)^2 \left(\frac{\pi\omega\varepsilon_0 n_1^2}{\beta}\right)\left(\frac{I_1(vR_1)}{J_1(uR_1)}\right)\left[\int_0^{R_1}\left\{R\left\{J_1(uR)\right\}^2\right\}dR\right] \tag{11}$$

$$p_{ic} = \Xi\left(\frac{\pi\omega\varepsilon_0 n_2^2}{\beta}\right)\left[\int_{R_1}^{R_2} R\left\{\Theta\left(\frac{I_1(vR_1)}{K_1(vR_1)}\right)K_1(vR)+I_1(vR)\right\}^2 dR\right] \tag{12}$$

$$p_{oc} = \Xi\left(\frac{\pi\omega\varepsilon_0 n_e^2}{\beta}\right)\left[\left(\frac{1}{K_1(qR_2)}\right)\left\{I_1(vR_2)+\Theta\left(\frac{K_1(vR_2)I_1(vR_1)}{K_1(vR_1)}\right)\right\}\right]^2 \left[\int_{R_2}^{\infty} R\left\{K_1(qR)\right\}^2 dR\right] \tag{13}$$

with $\Theta = \left(\frac{1-(n_1/n_2)^2}{(n_1/n_2)^2-1}\right)$.

In Eqs. (11)–(13), Ξ is a constant which may again be determined by the normalization condition considering the input power, and the new quantity q is defined as

$$q = \frac{n_o}{n_e}\sqrt{n_e^2 k_0^2 - \beta^2}. \tag{14}$$

Again the total power p_t transmitted by the TM_{01} modes through the liquid crystal fiber will be the sum of the power transported through the individual fiber sections, as given by Eqs. (11)–(13). Again, following the split-step method, the quantities R_1 and R_2 are, respectively, the localized values of the core and the inner clad radii of the fiber, and the values of β are throughout governed by Eq. (2).

3. RESULTS AND DISCUSSION

We now analyze the propagation characteristics of the liquid crystal tapered fiber under consideration in respected of the power transported by the transverse (TE and TM) modes through the different fiber sections. In our computation, we take the operating wavelength as 1.55 μm, and the RI values of core (i.e., n_1) and the inner clad (i.e., n_2) sections as 1.462 and 1.458, respectively. Further, the outermost clad with radially anisotropic nematic liquid crystal is taken to be a BDH mixture 14616 having the ordinary (i.e., n_o) and the extraordinary (i.e., n_e) RI values as 1.457 and 1.5037, respectively. As to the geometrical measurements of the tapered section, we take the taper length L as 5 cm with two different values of the inner core radius (10 μm and 30 μm) at the input end (i.e., $z = z_i$; Fig. 1), and a fixed value (100 μm) of the same at $z = z_o$.

Though this communication is basically aimed to highlight the propagation of power through different sections of the guide, it would be of worth to present a brief mention about the features of the dispersion behaviour. Figs. 3 and 4, respectively, illustrate the plots of the dispersion characteristics of the guide under the TE and TM mode excitations. The intersections of the curve with the horizontal axis will yield the allowed values of the modal propagation constants. We observe that the TE modes present more oscillatory behaviour than the TM modes. Further, the allowed values of the propagation constants correspond more to the case of TE mode excitation. The further details of the dispersion behaviour will be presented in a future communication.

Figures 5 and 6, respectively, correspond to the illustrations of the power carried by the transverse modes wherein the logarithmic plots of the power confinement factor are presented. At this point,

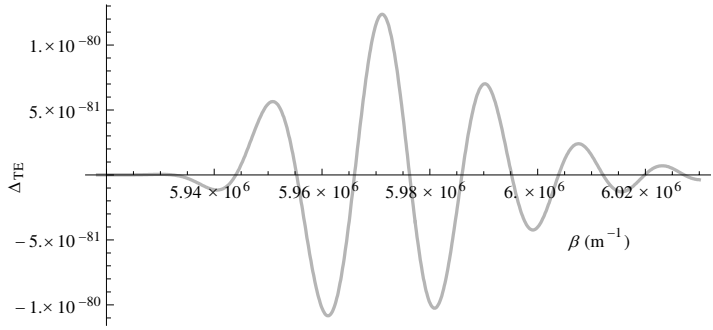

Figure 3. The dispersion behaviour of the guide under the TE mode excitation.

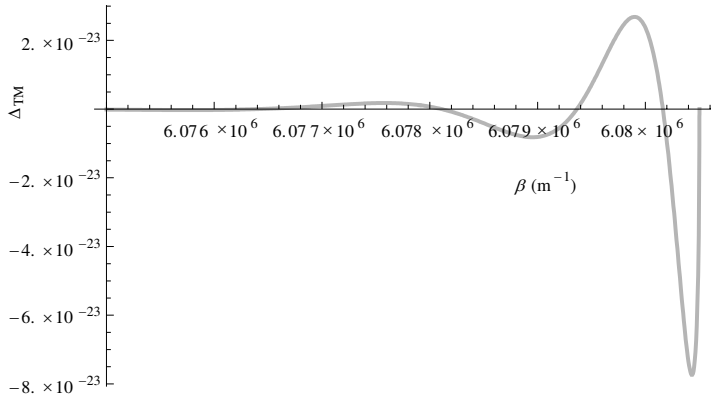

Figure 4. The dispersion behaviour of the guide under the TM mode excitation.

this is to be noted that, in the case of isotropic guides, the RI values remain independent of the direction of propagation giving thereby the identical values of the modal propagation constants and field cutoffs. As such, the transverse modes are very difficult to separate in the case of isotropic guides. In contrast, due to the direction-dependent RIs values for anisotropic guides (e.g., liquid crystal waveguides), the transverse modes in such guides will face different values of propagation constants, field cutoffs and dissimilar states of polarizations. However, the present communication is pivoted to the power transmitted by the tapered fiber having the outermost section as radially anisotropic nematic liquid crystal. Finally, an analytical investigation of the effect of using the amalgamation of tapered fiber loaded with radially anisotropic liquid crystal is touched upon.

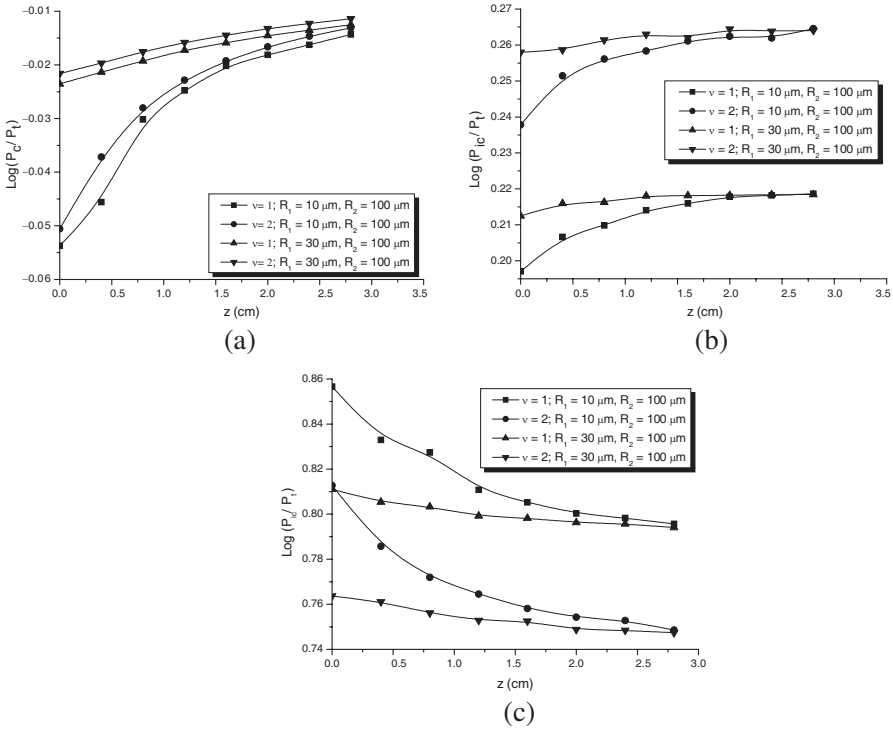

Figure 5. (a) TE mode power distribution in the tapered fiber core. (b) TE mode power distribution in the tapered fiber inner clad. (c) TE mode power distribution in the tapered fiber outer clad.

Figures 5(a), 5(b) and 5(c) illustrate the logarithmic plots of the relative power distributions in the tapered fiber core, the inner clad and the outermost liquid crystal clad, respectively, along the taper length, which is the direction of propagation too. As stated above, we consider two different values of the core radius of the input end, i.e., 10 μm and 30 μm, and the radius of the core output is taken as 100 μm. We observe that, in the fiber core (Fig. 5(a)), with the increase in taper length, the logarithmic power confinement also shows a gradual increase; the variation remains more pronounced corresponding to the lower input end dimension (i.e., 10 μm core radius). The phenomenon of gradual increase in power distribution is attributed to the fact that, as the wave propagates across the tapered region, there is a continuous increase in the waveguide dimension. A substantial increase in power is initially observed for the case of higher input end core radius, which is obviously due to the enhanced accumulation of power in this case. Further, for both the values of input core radius, the modes with higher

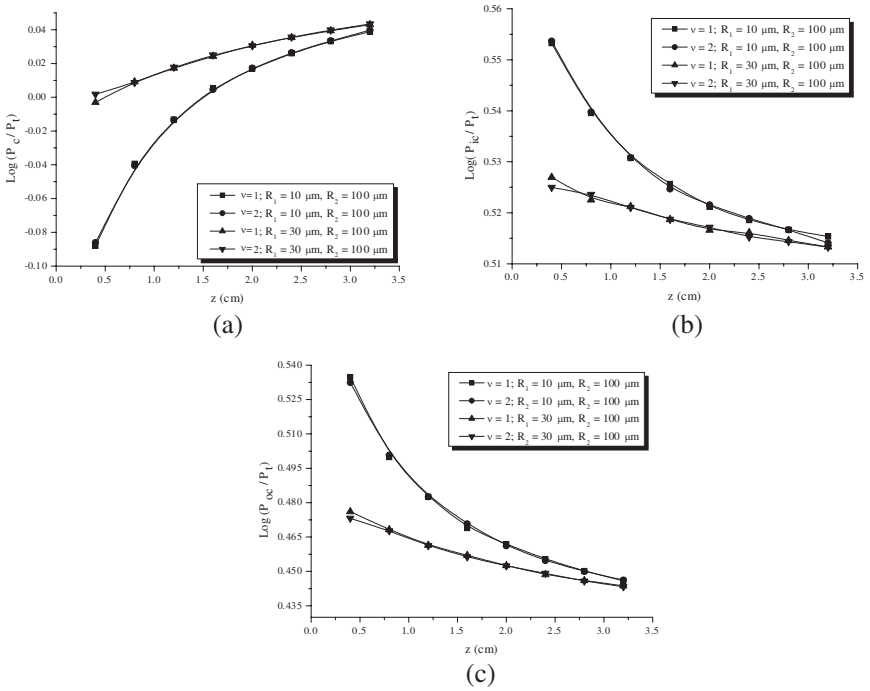

Figure 6. (a) TM mode power distribution in the tapered fiber core. (b) TM mode power distribution in the tapered fiber inner clad. (c) TM mode power distribution in the tapered fiber outer clad.

azimuthal index ($\nu = 2$) transport a little higher amount of power as compared to that by the lower azimuthal index value ($\nu = 1$).

In Fig. 5(b), we notice an almost similar behaviour (as in Fig. 5(a)) in the relative power distribution in the inner clad section with the only difference that the rise in power with taper length reaches a kind of saturation near the taper output region. However, a substantial increase in the transported power is found in this fiber section, and the attainment of saturation becomes quick corresponding to the fiber with larger dimension. Thus, it can be stated that the inner clad section sustains more amount of power than the fiber core.

A further pronounced enhancement in the transported power is seen in the outermost liquid crystal section wherein the relative power shows a very small decrease with the increase in taper length, and the decrease becomes more in the case of lower azimuthal index value, i.e., $\nu = 1$. Thus, the variation in the power confinement remains larger corresponding to the lesser value of the input core dimension; with the increase in input dimension, the confinement becomes almost

uniform without showing much change along the longitudinal taper length. This is attributed to the fact that the taper section undergoes larger variation in dimension along its length with smaller value of input end radius. The characteristic of attaining saturation is reversed in this fiber section.

Looking at the power confinements in all the three sections, the remarkable point to be observed is that, with the decrease of power in the fiber core or the inner clad, it simultaneously increases in the outermost liquid crystal clad, indicating thereby as if the power is *leaking off* the fiber core, and propagating through the clad sections. As such, the power is confined maximum in the radially anisotropic liquid crystal section, and this makes such fiber structures as promising candidates for sensing applications.

The aforesaid discussions correspond to the situation when the TE modes are excited in the tapered fiber. Now, considering the excitation of the TM modes, Figs. 6(a), 6(b) and 6(c) demonstrate the logarithmic variations of the power transmitted by the TM modes in the above discussed three regions of the fiber. The operating parameters are kept as the same we used in the case of TE mode power confinements.

We observe that, in all the fiber sections, the trend of power pattern with the taper length in the longitudinal direction (which is the direction of propagation too) remains almost the same as that previously noticed in the case of TE modes. However, the power carried by the modes of higher and the lower azimuthal index values are almost the same. Further, in the fiber core, the amount of overall transported power is slightly increased as compared to the case of TE modes (Fig. 5(a)). The same is observed in the inner clad as well — a substantial increase in the transmitted power is seen in this section as compared to the TE mode counterpart (Fig. 5(b)). However, compared to the case of TE modes (Fig. 5(c)), in the TM field excitation, not much increase in power is demonstrated in the outermost liquid crystal clad. Apart from all these, we find the highest amount of power being propagated in the inner clad, which is in contrast to the situation observed in the case of TE modes wherein the maximum amount of power is observed to be sustained in the outermost clad. In the present case, we observe the power confinement in the outermost liquid crystal region (Fig. 6(c)) to be is slightly less than that in the inner clad. As such, corresponding to the TM mode excitation, the maximum amount of power is sustained in the inner clad region of the fiber, whereas the outermost clad confines slightly less amount of power than the inner clad; the fiber core region certainly sustains the minimum amount of power.

4. CONCLUSION

From the foregoing discussions, it can be inferred that, in tapered fibers with radially anisotropic liquid crystal outer clad, the TE modes transport the maximum amount of power in the outermost region. This feature is not that strong corresponding to the TM mode excitation as the confinement remains mostly in the inner clad region in this case. It is noticeable that the higher amount of power distribution in clad sections can be interpreted as if the power is *leaking off* the fiber core, and transferred to the fiber clad – the feature strongly observed in the case of TE mode excitation. Further, this phenomenon is attributed to the presence of radially anisotropic liquid crystal in the outermost clad. Apart from this, the taper geometry also plays its role to transfer power to the outer clad. As such, an amalgamation of the taper structure and the clad anisotropy brings in an enhanced power in the outer clad region — a much desirable characteristics for optical sensing and field coupling devices.

Further work in this direction is in progress and will be taken up in a future communication.

ACKNOWLEDGMENT

One of the authors (PKC) is thankful to Prof. Burhanuddin Yeop Majlis for constant encouragement and help. Fruitful suggestions by Prof. S. Shaari are also gratefully acknowledged. The authors are immensely grateful to the two anonymous reviewers for constructive criticisms to enhance the status of the manuscript. Also, they are thankful to Patrick Teh Swee Ping for some computational helps.

REFERENCES

1. Le Floch, J. M., F. Houndonougbo, V. Madrangeas, D. Cros, M. Guilloux-Viry, and W. Peng, "Thin film materials characterization using TE modes cavity," *Journal of Electromagnetic Waves and Applications*, Vol. 23, No. 4, 549–559, 2009.
2. Siong, C. C. and P. K. Choudhury, "Propagation characteristics of tapered core helical clad dielectric optical fibers," *Journal of Electromagnetic Waves and Applications*, Vol. 23, No. 14–15, 663–674, 2009.
3. Xu, J., W. X. Wang, L. N. Yue, Y. B. Gong, and Y. Y. Wei, "Electromagnetic wave propagation in an elliptical chiroferrite waveguide," *Journal of Electromagnetic Waves and Applications*, Vol. 23, No. 14–15, 2021–2030, 2009.

4. Wu, Z., B. Q. Zeng, and S. Zhong, "A double-layer chiral metamaterial with negative index," *Journal of Electromagnetic Waves and Applications*, Vol. 24, No. 7, 983–992, 2010.
5. Seo, D.-W., H.-J. Kim, K.-U. Bae, and N.-H. Myung, "The effect of fiber orientation distribution on the effective permittivity of fiber composite materials," *Journal of Electromagnetic Waves and Applications*, Vol. 24, No. 17–18, 2419–2430, 2010.
6. Choudhury, P. K. and D. Kumar, "On the slow-wave helical clad elliptical fibers," *Journal of Electromagnetic Waves and Applications*," Vol. 24, No. 14–15, 1931–1942, 2010.
7. Noor Amin, A. S., M. Mirhosseini, and M. Shahabadi, "Modal analysis of multilayer conical dielectric waveguides for azimuthal invariant modes," *Progress In Electromagnetics Research*, Vol. 105, 213–229, 2010.
8. Chen, D. and B. Sun, "Multi-wavelength fiber optical parametric oscillator based on a highly nonlinear fiber and a sagnac loop filter," *Progress In Electromagnetics Research*, Vol. 106, 163–176, 2010.
9. Tuz, V. R. and C.-W. Qiu, "Semi-infinite chiral nihility photonics: Parametric dependence, wave tunneling and rejection," *Progress In Electromagnetics Research*, Vol. 103, 139–152, 2010.
10. Ahmed, S. and Q. A. Naqvi, "Electromagnetic scattering from a chiral-coated nihility cylinder," *Progress In Electromagnetics Research Letters*, Vol. 18, 41–50, 2010.
11. Baqir, M. A., A. A. Syed, and Q. A. Naqvi, "Electromagnetic fields in a circular waveguide containing chiral nihility metamaterial," *Progress In Electromagnetics Research M*, Vol. 16, 85–93, 2011.
12. Kesari, V. and J. P. Keshari, "Analysis of a circular waveguide loaded with dielectric and metal discs," *Progress In Electromagnetics Research*, Vol. 111, 253–269, 2011.
13. Dong, J.-F., J. Li, and F.-Q. Yang, "Guided modes in the four-layer slab waveguide containing chiral nihility core," *Progress In Electromagnetics Research*, Vol. 112, 241–255, 2011.
14. Sage, I. and D. Chaplin, "Low RI liquid crystals for integrated optics," *Electron. Lett.*, Vol. 23, 1192–1193, 1987.
15. Kashyap, R., C. S. Winter, and B. K. Nayar, "Polarization desensitized liquid-crystal overlay optical-fiber modulator," *Opt. Lett.*, Vol. 13, 401–403, 1988.
16. Ioannidis, Z. K., I. P. Giles, and C. Bowry, "All-fiber optic intensity modulators using liquid crystals," *Appl. Opt.*, Vol. 30,

328–333, 1991.

17. Wu, S.-T. and U. Efron, "Optical properties of thin nematic liquid crystal cells," *Appl. Phys. Lett.*, Vol. 48, 624–636, 1986.
18. Goldburt, E. S. and P. S. J. Russell, "Electro-optical response of a liquid-crystalline fiber coupler," *Appl. Phys. Lett.*, Vol. 48, 10–12, 1986.
19. Chen, S.-H. and T.-J. Chen, "Observation of mode selection in a radially anisotropic cylindrical waveguide with liquid-crystal cladding," *Appl. Phys. Lett.*, Vol. 64, 1893–1895, 1994.
20. Ono, K. and H. Osawa, "Excitation characteristics of fundamental mode in tapered slab waveguides with nonlinear cladding," *Electron. Lett.*, Vol. 27, 664–666, 1991.
21. Lim, M. H., S. C. Yeow, P. K. Choudhury, and D. Kumar, "Towards the dispersion characteristics of tapered core dielectric optical fibers," *Journal of Electromagnetic Waves and Applications*, Vol. 20, No. 12, 1597–1609, 2006.
22. Yeow, S. C., M. H. Lim, and P. K. Choudhury, "A rigorous analysis of the distribution of power in plastic clad linear tapered fibers," *Optik*, Vol. 117, 405–410, 2006.
23. Choudhury, P. K. and D. Kumar, "Towards dispersion relations for tapered core dielectric elliptical fibers," *Optik*, Vol. 118, 340–344, 2007.
24. Choudhury, P. K. and T. Yoshino, "TE and TM modes power transmission through liquid crystal optical fibers," *Optik*, Vol. 115, 49–56, 2004.
25. Choudhury, P. K. and T. Yoshino, "On the propagation of power through liquid crystal clad optical fibers," *Proc. SPIE*, Vol. 5560, 380–385, 2004.
26. Choudhury, P. K. and W. K. Soon, "TE mode propagation through tapered core liquid crystal optical fibers," *Progress In Electromagnetic Research*, Vol. 104, 449–463, 2010.
27. Choudhury, P. K. and O. N. Singh, "Some multilayered and other unconventional lightguides," *Electromagnetic Fields in Unconventional Structures and Materials*, 289–357, O. N. Singh, A. Lakhtakia, Eds., John Wiley, New York, 2000.
28. Snyder, A. W. and F. Rühl, "Single-mode, single-polarization fibers made of birefringent material," *J. Opt. Soc. Am.*, Vol. 73, 1165–1174, 1983.